

Turbulence in Core-Collapse Supernovae

David Radice^{1,2}, Ernazar Abdikamalov³, Christian D. Ott⁴,
 Philipp Mösta^{5†}, Sean M. Couch^{6,7,8}, and
 Luke F. Roberts^{6,8}.

¹ School of Natural Sciences, Institute for Advanced Study, 1 Einstein Drive, Princeton, NJ 08540, USA

² Department of Astrophysical Sciences, 4 Ivy Lane, Princeton University, Princeton, NJ 08544, USA

³ Department of Physics, School of Science and Technology, Nazarbayev University, Astana 010000, Kazakhstan

⁴ TAPIR, Walter Burke Institute for Theoretical Physics, Mailcode 350-17, California Institute of Technology, Pasadena, CA 91125, USA

⁵ Department of Astronomy, 501 Campbell Hall #3411, University of California at Berkeley, Berkeley, California 94720, USA

⁶ Department of Physics and Astronomy, Michigan State University, East Lansing, MI 48824, USA

⁷ Department of Computational Mathematics, Science, and Engineering, Michigan State University, East Lansing, MI 48824, USA

⁸ National Superconducting Cyclotron Laboratory, Michigan State University, East Lansing, MI 48824, USA

Abstract. Multidimensional simulations show that non-radial, turbulent, fluid motion is a fundamental component of the core-collapse supernova (CCSN) explosion mechanism. Neutrino-driven convection, the standing accretion shock instability, and relic-perturbations from advanced stages of nuclear burning can all impact the outcome of core collapse in a qualitative and quantitative way. Here, we review the current understanding of these phenomena and their role in the explosion of massive stars. We also discuss the role of protoneutron star convection and of magnetic fields in the context of the delayed neutrino mechanism.

1. Introduction

The formation of an iron core at the center of evolved massive stars, i.e., with zero-age main-sequence masses of $\sim 10 M_{\odot}$ or more, is a robust prediction of stellar evolution theory. It is also well established that, once it reaches a critical mass of $\sim 1.4 M_{\odot}$, the iron core becomes dynamically unstable and succumbs to its self-gravity. The collapse proceeds until the center reaches nuclear density $\simeq 2.7 \times 10^{14} \text{ g cm}^{-3}$. Then, the equation of state (EOS) stiffens because of the repulsive component of the strong nuclear force. The inner part of the iron core, that is in sonic contact during the collapse, halts its contraction and bounces back. A protoneutron star (PNS) is thus formed. The outer part of the iron core, that is infalling supersonically, rams into it producing a strong shock wave.

In the case of the most common variety of core-collapse supernovae (CCSNe), this shock wave is expected to expand toward the stellar surface, depositing energy

† NASA Einstein Fellow

and unbinding material, ultimately powering the explosion. However, this process is far from straightforward. Within ~ 20 ms of its formation, the shock wave loses about two Bethes ($1B \equiv 10^{51}$ erg) of energy due to the neutrino shock-breakout burst. Subsequently, as the shock moves out in mass, it loses energy at the rate of 8.8 MeV per nucleon (~ 1.7 B per $0.1 M_\odot$) as it dissociates iron-group nuclei into free nucleons. Eventually, within a few tens of milliseconds, the shock stalls and turns into a standing accretion shock stagnating at a radius between 100 and 200 kilometers. For the explosion to be successful, some physical mechanism must revive the shock within a timescale of ~ 1 second. Otherwise, the PNS would collapse to form a black hole. Understanding this mechanism is one of the most pressing problems in astrophysics.

The leading theoretical model for shock revival is the so-called delayed neutrino mechanism [1, 2]. According to this mechanism, it is the absorption of neutrinos radiated from the PNS and its cooling mantle that revives the shock. All modern simulations show the formation of a layer behind the shock, the so-called gain region, with net neutrino heating. Whether this is the mechanism solely responsible for the explosion is still uncertain. For instance, we now know that for most progenitors the delayed neutrino mechanism does not work in spherical symmetry [3–8]. However, successful explosions have been obtained in multiple dimensions thanks to the presence of hydrodynamical instabilities, such as the standing accretion shock instability (SASI) [9, 10] and neutrino-driven convection [11–14]. These instabilities break the spherical symmetry of the problem and generate turbulence. These two effects, asphericities of the flow and turbulence, are now recognized as being crucial for successful explosions. Indeed, as shown in Fig. 1, turbulence is present over most of the region interior to the shock.

The kinematic viscosity in the region immediately below the shock is dominated by neutron scattering and is very small, implying extremely high Reynolds-number flow ($Re \approx 10^{17}$; [15]). An important ramification for radiation-hydrodynamics CCSN simulations is that they need to be 3D and have sufficiently high resolution to capture the turbulent flow in the implicit large eddy simulation (ILES) paradigm [16–18]. In 1D (spherical symmetry) there is only radial flow. In 2D (axisymmetry), turbulence exhibits an inverse cascade that transfers kinetic energy to large scales [19] where it can artificially help the explosion [20–22].

The purpose of this article is to review our current understanding of the role of turbulence and other fluid instabilities in the explosion mechanism of CCSNe. We refer to the recent reviews by [29–32] for more broad overviews of CCSN theory. The rest of this article is organized as follows. In Section 2, we focus on the development of neutrino-driven convection and its role in the explosion mechanism. Section 3 is dedicated to the SASI. In Section 4, we consider the evolution of perturbations, originating in convective nuclear burning shells, as they are advected and amplified during core collapse. We discuss in more detail the role that pre-SN perturbations can have in aiding the explosion in Section 5. Section 6 is dedicated to the role of PNS convection. We review the possible role of magnetohydrodynamic (MHD) effects for the explosion of regular CCSNe in Section 7. Finally, we conclude in Section 8 with a brief summary and a discussion of future prospectives in the study of turbulence in CCSNe.

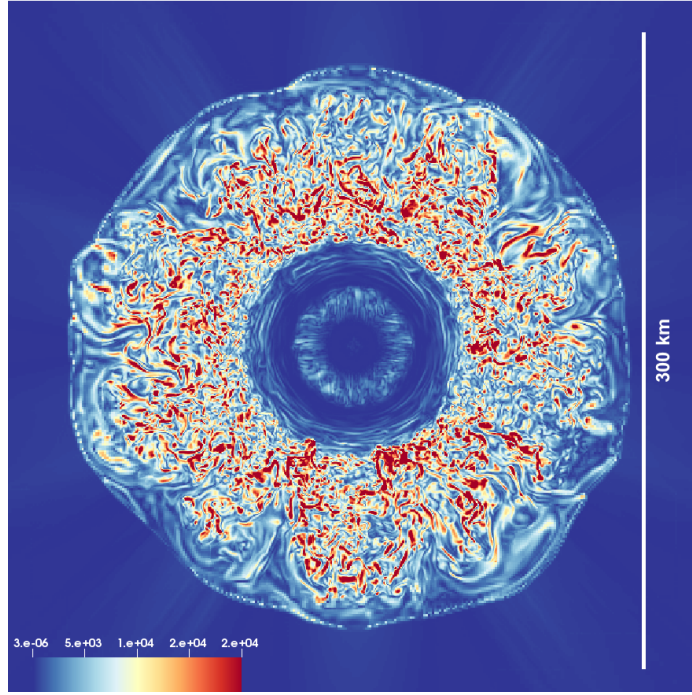


Figure 1. Regions of intense vorticity during the stalled-shock phase of the explosion of a CCSN. The color code shows the amplitude of the vorticity. The data are taken at 210 milliseconds after bounce for a $20-M_{\odot}$ progenitor. The progenitor model was computed with MESA [23, 24], while the simulation was performed in 3D using the FLASH code with M1 neutrino transport [25–27]. Turbulent convection immediately behind the shock is clearly visible and is characterized by the presence of small tubular structures with intense vorticity. Similar structures are known to characterize incompressible turbulence in periodic domains [28]. The vortical structures near the core are due to PNS convection.

2. Neutrino-Driven Convection

2.1. The Development of Convection

Because of the geometric dilution of the neutrino radiation field, the net heating rate per baryon has a maximum within the gain layer and decreases outwards. This naturally leads to the formation of an unstable (negative) entropy gradient. The gain region is unstable to convection according to both the Schwarzschild [33] and the Ledoux [34] criteria.

According to the Ledoux criterion, in the case of a static background, the growth rate of small convective eddies is given by the imaginary part of the Brunt-Väisälä frequency:

$$\Omega_{\text{BV}}^2 = \frac{g}{\rho} \left(\frac{\partial \rho}{\partial p} \right)_{s, Y_e} \left[\left(\frac{\partial p}{\partial s} \right)_{\rho, Y_e} \frac{\partial s}{\partial r} + \left(\frac{\partial p}{\partial Y_e} \right)_{\rho, s} \frac{\partial Y_e}{\partial r} \right], \quad (1)$$

where the electron fraction Y_e is used to express the composition of the flow, s is its entropy per baryon, and g is the gravitational acceleration.

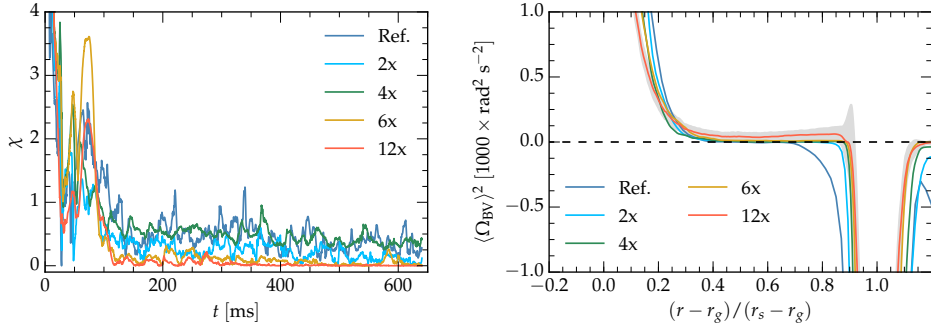


Figure 2. Left panel: evolution of Foglizzo’s χ , Eq. (2). Right panel: time and angle averaged Brunt-Väisälä frequency Ω_{BV} as a function of a normalized radial coordinate. The results are from the 3D high-resolution, semi-global, parameterized, neutrino-driven convection simulations presented in [18]. Here, χ is computed from the angle-averaged Ω_{BV} and velocity, r_g is the radius at which the angle-averaged net neutrino heating rate first becomes positive, and r_s is the shock radius. The initial value of χ is 5.33, but it drops significantly once convection is fully developed and $\langle \Omega_{\text{BV}} \rangle^2$ is positive over most of the gain region. The final value of χ also decreases with resolution.

Classically, as soon as $\Omega_{\text{BV}}^2 < 0$ convection is expected to develop. However, as pointed out by Foglizzo et al. [14], in the case of the gain layer in CCSNe, there is an additional condition that needs to be satisfied for convection to develop: the growth rate of the convective instability must be large enough to ensure that buoyant plumes can grow sufficiently before being advected out of the gain region. This condition is expressed in terms of the non-dimensional parameter

$$\chi = \int \frac{|\Omega_{\text{BV}}|}{|v_r|} dr, \quad (2)$$

where the integral is restricted to those regions of the gain layer where Ω_{BV}^2 is negative. χ can be interpreted as the number of e-folding times experienced by a buoyant perturbation before being accreted into the cooling layer above the PNS. Many numerical simulations have shown that, when $\chi \gtrsim 3$, convection develops [14, 15, 22, 35–42]. On the other hand, the interpretation of χ in the presence of large deviations of the background flow from spherical symmetry is less clear. First, since Eq. (2) is non-linear, computing χ using angle and time averaged flow variables gives results that can be significantly different from its direct evaluation as a volume integral [39]. This is because, in this case, the value of χ can be dominated by points with small radial velocities. Differences are also likely to arise depending on whether χ is computed using the average Brunt-Väisälä frequency, e.g., [39], or the Brunt-Väisälä frequency of the averaged flow, e.g., [40]. Second, numerical simulations suggest that in the presence of sufficiently large perturbations convection might develop also for small values of χ [35, 43]. Finally, once convection is fully developed, χ often decreases to below the critical value of three [22, 39].

For example, Fig. 2 shows that if χ is computed from the angle averaged Ω_{BV} and radial velocity, then the development of convection tends to drive χ toward zero. In particular, the left panel Fig. 2 shows the evolution of χ from a series of parametrized semi-global neutrino driven convection simulations [18]. The reference resolution is $\Delta r \simeq 3.8$ km and $\Delta\phi = \Delta\theta = 1.8^\circ$. The other simulations have their resolution

increased (grid spacing decreased) by factors 2, 4, 6, and 12. The initial value of χ is 5.33, but, as soon as convection is fully developed, χ drops significantly and it reaches essentially zero in the highest resolution runs. Despite the vanishing value of χ , convection is fully developed for the entire duration of the simulations. However, the flow re-arranges so that $\langle \Omega_{BV} \rangle^2 \gtrsim 0$ almost everywhere in the gain layer (right panel of Fig. 2). The only exceptions are the points where the angle averaging crosses the shock surface and $\langle \Omega_{BV} \rangle$ is not particularly meaningful (these points are not considered when computing χ from Eq. [2]).

Clearly, the interpretation of Foglizzo's χ once the flow has broken the spherical symmetry is difficult and its value is not necessarily indicative of whether convection or SASI is dominating. On the other hand, the value of χ shortly after bounce is predictive of the onset of convection. Foglizzo's criterion also shows that convection should become dominant for models with low accretion rates and/or high neutrino luminosities. This has been extensively confirmed by many 3D simulations, e.g., [15, 20, 22, 36, 40, 43–50].

2.2. The Impact of Convection

The importance of convection in the gain layer below the shock has been recognized for many years, see e.g., [51]. The results from some of the earliest multi-dimensional (2D) simulations suggested that convection might be strong enough to trap energy into the gain region [11, 52]. According to these simulations, the temperature of the gas below the shock would then continuously increase due to neutrino absorption until a critical threshold after which the explosion would set in. This was the so-called convective engine model. However, the results from more advanced simulations, e.g., starting from [12, 13], questioned these earlier studies and showed that the impact of convection is important, but more subtle.

Modern simulations show that once convection develops, a new equilibrium is typically reached with no net accumulation of mass or energy in the gain region. Instead, the explosion, if successful, is likely to develop in a more nuanced way if the right conditions, often expressed in terms of neutrino energy deposition and accretion rate [53], are met. In other words, neutrino-driven convection is not able to completely trap material in the gain region and create a run-away accumulation of energy. However, it can aid the explosion by creating more favorable conditions for the shock to run away, for instance, when the accretion rate suddenly drops as compositional interfaces cross the shock.

One way convection aids the explosion is by entraining some of the gas, which, as a consequence, has more time to absorb neutrinos [12, 44, 54, 55]. Equivalently, convection decreases the typical advection timescale

$$t_{\text{adv}} = \frac{M_{\text{gain}}}{\dot{M}}, \quad (3)$$

bringing it closer to the timescale needed to heat the material in the gain region sufficiently to unbind it [56–58].

Another possibility is that if convection is sufficiently strong, it could drive a redistribution of entropy leading to conditions that are more favorable for explosion [51]. This effect was quantified by Yamasaki & Yamada [59] in terms of its reduction on the critical neutrino luminosity [53], the neutrino luminosity beyond which the shock is able to overcome the ram pressure of the accreting material.

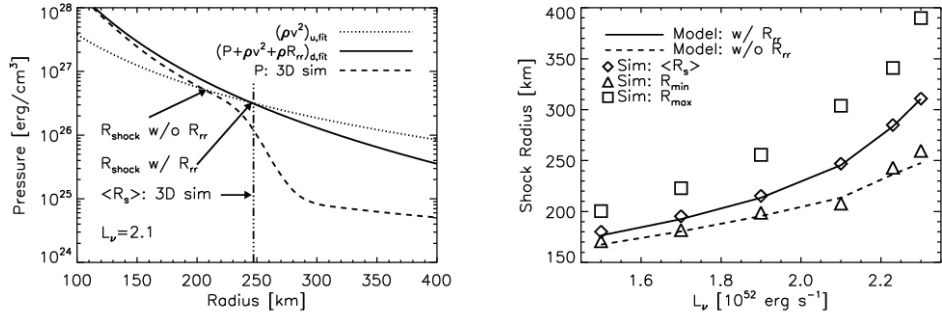


Figure 3. Left panel: power-law fits of the upstream and downstream components of Eq. (5). The location of the average shock radius $\langle R_s \rangle$ and of the predictions from Eq. (4), which does not account for the turbulent pressure, and from Eq. (5), which includes the effect of turbulent pressure, are also indicated. Right panel: minimum, maximum, and average shock radii in parametrized 3D simulations of neutrino-driven convection with different neutrino luminosities. Also shown are the predictions from Eqs. (4) and (5). Reprinted from J. Murphy, J. Dolence, and A. Burrows, *The Dominance of Neutrino-Driven Convection in Core-Collapse Supernovae*, The Astrophysical Journal **771**, 52 (2013) [45], © AAS. Reproduced with permission.

They showed that if convection is able to suppress the radial gradient of the angle-averaged specific entropy, then the critical luminosity is effectively decreases by a factor of two. On the other hand, simulations have shown that, in conditions typical of CCSNe, neutrino-driven convection is not sufficiently vigorous to realize the scenario hypothesized by Yamasaki & Yamada [18, 37, 43, 44, 60, 61] and the reduction in the critical neutrino luminosity is smaller than what they predicted.

Neutrino-driven convection behind the shock is turbulent and the chaotic motion of the fluid can result in an effective additional pressure support behind the stalled shock. This was first pointed out by Murphy et al. [45] and later confirmed and extended by Couch & Ott [21] and by Radice et al. [18]. Following the original argument by Murphy et al. [45], we consider the Rankine-Hugoniot momentum condition for a standing accretion shock,

$$\rho_d v_d^2 + p_d = \rho_u v_u^2 + p_u, \quad (4)$$

where ρ is the density, v the radial velocity, and p the pressure. We have also denoted with \cdot_d and \cdot_u the downstream and upstream quantities respectively.

In the presence of turbulence, [45] suggested to modify equation (4) in a way akin to a Reynolds decomposition and write it as

$$\rho_d v_d^2 + \rho_d R_{rr} + p_d = \rho_u v_u^2 + p_u, \quad (5)$$

where R_{rr} is the radial component of the Reynolds stress tensor,

$$R_{ij} = \langle \delta v_i \delta v_j \rangle, \quad (6)$$

and δv_i is the difference between the fluid velocity and the angle-averaged radial velocity of the flow. Although not entirely rigorous, Eq. (5) has been shown to be well verified in numerical simulations if angular averages are used to compute the respective quantities [18, 21, 45, 62]. This is shown in Fig. 3, reproduced from Murphy et al. [45]. There, the shock location in 3D parametrized neutrino-driven convection simulations

is compared with the prediction from Eq. (5). As can be seen in Fig. 3, the effective pressure support generated by the turbulence accounts for an increase in the shock radius of $\sim 25\%$ [45]. Furthermore, Couch & Ott [21] showed that the effective pressure support due to turbulence can be as large as $\sim 50\%$ of the thermal pressure.

Couch & Ott [21] also showed that the transition to explosion in CCSNe is associated with an increase in the total turbulent energy in the gain region, defined as

$$E_{\text{turb}} = \frac{1}{2}\rho|\delta\mathbf{v}|^2. \quad (7)$$

The importance of turbulent energy can be better understood by recasting Eq. (5), following [63]

$$\rho_d v_d^2 + (\gamma_{\text{th}} - 1)\rho_d \epsilon_{\text{th}} + (\gamma_{\text{turb}} - 1)\rho_d \epsilon_{\text{turb}} = \rho_u v_u^2 + p_u, \quad (8)$$

where ϵ_{th} is the specific internal energy downstream of the shock, $\gamma_{\text{th}} \simeq 4/3$ is the adiabatic index for a radiation pressure dominated gas, and $\epsilon_{\text{turb}} = E_{\text{turb}}/\rho_d$ is the specific turbulent energy density. γ_{turb} is an effective adiabatic index which is equal to $5/3$ for isotropic turbulence and to 2 for anisotropic turbulence with $R_{rr} \simeq R_{\theta\theta} + R_{\phi\phi}$. The latter case is commonly realized in convection simulations, e.g., [18, 21, 45, 64], and should be the relevant case for CCSNe. Equation (8) illustrates that turbulent kinetic energy contributes to the overall pressure support behind the shock. More importantly, since $\gamma_{\text{turb}} > \gamma_{\text{th}}$, Eq. (8) shows that turbulent kinetic energy is a more “valuable” form of energy than thermal energy. The ratio $\epsilon_{\text{turb}}/\epsilon_{\text{th}}$ is then a crucial quantity for the revival of the shock.

Another formulation of Eq. (8) was proposed by Müller & Janka [62]. Instead of the turbulent energy, they computed the turbulent pressure from the rms Mach number of the turbulence

$$\langle \mathcal{M}^2 \rangle = \frac{2E_{\text{kin},\theta}}{M_{\text{gain}}c_{s,d}^2} \simeq \frac{\epsilon_{\text{turb}}}{c_{s,d}^2}, \quad (9)$$

$c_{s,d}$ being the sound speed downstream of the shock. With this definition the total pressure support behind the shock (turbulent plus thermal) is given by

$$p = p_{\text{th}}(1 + \gamma_{\text{th}}\langle \mathcal{M}^2 \rangle) \simeq p_{\text{th}} \left(1 + \frac{4}{3}\langle \mathcal{M}^2 \rangle\right). \quad (10)$$

Radice et al. [18] presented a more formal derivation of Eq. (5), which they reformulated as a global integral condition implicitly determining the location of the shock. Their analysis confirmed the previous interpretation of the importance of the effective turbulent pressure. Furthermore, they found that the non-radial fluid motion due to turbulence also contributes significantly to the effective pressure support of the flow. This is because, even though the angular momentum of the flow is conserved, the fluid still experiences a net centrifugal force.

More recently, Mabant & Murphy [65] considered the impact of turbulence on the explosion conditions using a new semi-analytic model. They extended the work of Yamasaki & Yamada [59] by combining the neutrino-driven convection model developed by Murphy & Meakin [61] with the steady-state model of Murphy & Dolence [66]. They pointed out that neutrino-driven convection is able to tap into the gravitational potential energy associated with the unstable stratification of the material behind the shock. According to their model, buoyancy would transform this potential energy into kinetic energy, which would then be transformed into thermal

energy by turbulent dissipation. Mabanta & Murphy [65] argued that the subsequent enhanced thermalization of the flow would be the most important consequence of turbulence for the explosion mechanism of CCSNe. However, this effect has not yet been investigated using multi-dimensional simulations, so its quantitative impact remains unclear.

Clearly, all of the effects of neutrino-driven convection just discussed are deeply connected. The increased residence time of fluid elements in the gain region, the convective luminosity, the turbulent dissipation, and the effective turbulent pressure support, can all be described using the Reynolds decomposition, e.g., [18, 61], of the mass, energy, and momentum conservation equations respectively.

2.3. Turbulent Energy Cascade

On the basis of the previous discussion, we can conclude that the ratio between turbulent and thermal pressure is an important parameter affecting the dynamics of the shock revival in neutrino-driven CCSNe. This ratio in turn is set by the efficiency with which kinetic energy is transferred to small scales by the turbulence cascade, where it is dissipated into heat. Understanding how the turbulent cascade operates in neutrino-driven convection and how well it is captured in finite-resolution simulations is important to be able to quantify the role of turbulence in the explosion and the fidelity of the numerical models.

The turbulent energy spectrum is the main diagnostic used to study the turbulent cascade [15, 21, 22, 37, 44, 46, 67, 68]. Most investigators focused on the transverse turbulent spectrum

$$E(\ell) = \sum_{m=-\ell}^{\ell} \left| \int \sqrt{\rho} v_t Y_\ell^m d\Omega \right|^2, \quad (11)$$

where Y_ℓ^m are the spherical harmonics, v_t is the non-radial part of the velocity, and the integral is evaluated on a shell at a fixed radius. Another quantity of interest is the specific turbulent energy spectrum

$$E(k) = \frac{1}{2} \sum_{i=1}^3 \int_{\mathbb{R}^3} \delta(|\mathbf{k}| - k) \widehat{\delta v_i^*}(\mathbf{k}) \widehat{\delta v_i}(\mathbf{k}) d\mathbf{k}, \quad (12)$$

where $\widehat{\cdot}$ is the Fourier transform, defined as

$$\widehat{\delta v_i}(\mathbf{k}) = \int_{\mathbb{R}^3} \delta v_i(\mathbf{x}) e^{2\pi i \mathbf{k} \cdot \mathbf{x}} d\mathbf{x} \quad (13)$$

and \cdot^* denotes the complex conjugation. Finally, δv_i is defined as in Eq. (6). Apart from the normalization factor, this quantity coincides with the velocity power-spectrum, which is also the Fourier transform of the two-point correlation function of the velocity [69].

At scales that are well separated from those at which turbulence is driven by neutrinos and dissipated by microphysical processes, the statistical properties of turbulence in steady state, including the spectra, are expected to be universal [69]. At these intermediate scales, in the so-called inertial range, the spectra $E(\ell)$ and $E(k)$ should become self-similar power laws [69]. For example, in Kolmogorov's classical theory of turbulence $E(k) \propto k^\alpha$ with index $\alpha = -5/3$. Note that, in the limit of large ℓ , and since $\rho \simeq \text{const}$ at a fixed radii, $E(k) \propto k^\alpha$ is equivalent to $E(\ell) \propto \ell^\alpha$, e.g., [70], chapter 21.

In the phenomenology associated with Kolmogorov's theory the energy flux across scales is constant in the inertial range. Consequently, the energy dissipation rate in well developed turbulence only depends on the large scale dynamics, which provides the “inflow” boundary condition for the energy transport to small scale. Consequently, the presence of a well resolved inertial range is regarded as a sufficient condition to ensure that a numerical simulation is capturing the turbulent dissipation of energy from the largest eddies.

One possible issue is that Kolmogorov's theory of turbulence may not necessarily apply to neutrino-driven convection. Indeed, turbulence in the postshock region of CCSNe is anisotropic, as gravity breaks the local rotational symmetry of the fluid equations [18, 21, 45, 61, 68], mildly compressible (reaching pre-explosion Mach numbers of $\simeq 0.3 - 0.5$ [71, 72]), and driven at multiple scales by buoyancy.

Anisotropic and mildly compressible flows have been shown to still follow Kolmogorov's theory, e.g. [63, 73, 74]. The effect of buoyancy has been considered by Goldreich & Keeley [75] who argued that Kolmogorov's phenomenology should still apply, because turbulent stresses become dominant over buoyancy forces at sufficiently small scales. Here, we present a revised and generalized version of their argument.

Consider eddies with typical size l (not to be confused with the spherical harmonic index ℓ), s.t. $\eta \ll l \ll L$, where L is the energy injection scale, i.e., the size of the gain region, and η is the dissipation scale. The buoyancy forces acting on these eddies scale as the entropy fluctuations at the scale of the eddies:

$$F_l^B \sim \delta s_l. \quad (14)$$

Inertial forces scale as[§]

$$F_l^I \sim \frac{(\delta v_l)^2}{l}. \quad (15)$$

Let us assume that velocity and entropy fluctuations scale as power laws of l ||

$$(\delta v_l)^2 \sim l^{2\beta}, \quad \delta s_l \sim l^\gamma. \quad (16)$$

Note that from Eq. (12) and the properties of the Fourier transform, it follows that the power-spectrum of the velocity is also a power law with index $\alpha = -2\beta - 1$, e.g., [69]. Under these assumptions, the ratio between inertial and buoyant forces acting on eddies with typical scale l is

$$\frac{F_l^I}{F_l^B} \sim l^{2\beta-\gamma-1}, \quad (17)$$

which shows that inertial forces dominate on sufficiently small scales as long as

$$2\beta < \gamma + 1. \quad (18)$$

This condition is verified for turbulence with Kolmogorov's spectrum, where $\beta = \gamma = 1/3$ suggesting that a flow satisfying Eq. (18) will develop a Kolmogorov spectrum at scales $\eta \ll l \ll l^*$, l^* being the scale at which $F_{l^*}^I \sim F_{l^*}^B$ over one eddy turnover timescale $\tau_l = l/\delta v_l$.

We stress that Eq. (18) is satisfied for most values of β and γ in the physically relevant range $0 < \beta, \gamma < 1$ (note that $\beta \geq 1$ or $\gamma \geq 1$ would imply smooth, laminar velocity or entropy fields, respectively, e.g., [69]). On the basis of this argument, we can conclude that buoyancy should become negligible at small scales $l \ll l^*$ and

[§] Note that these are a manifestation of the $(\mathbf{v} \cdot \nabla) \mathbf{v}$ term in the Euler's equations.

|| Equivalently, we assume the existence of an inertial range.

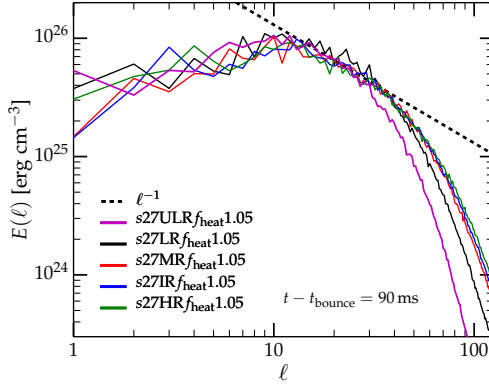


Figure 4. Transverse energy spectra at different resolutions for one of the models from Abdiakamalov et al. [15]. Note that the spectra have a rather shallow ℓ^{-1} dependency at intermediate scales of $10 \lesssim \ell \lesssim 40$. Reprinted from E. Abdiakamalov, C. D. Ott, D. Radice, L. F. Roberts, R. Haas, C. Reisswig, P. Mösta, H. Klion, and E. Schnetter, *Neutrino-Driven Turbulent Convection and Standing Accretion Shock Instability in Three-Dimensional Core-Collapse Supernovae*, The Astrophysical Journal **808**, 70 (2015) [15], © AAS. Reproduced with permission.

deviations from Kolmogorov scaling should not be expected, unless compressibility or other non-ideal effects become important, or Eq. 18 is violated.

Hanke et al. [37] claimed to observe a turbulent energy spectrum with $\alpha \simeq -5/3$. Similar results were later reported by Handy et al. [68] and Summa et al. [76]. However, later simulations employing Cartesian grids and higher resolutions found shallower power-spectra with $\alpha \simeq -1$ [15, 21, 22, 44]. See Fig. 4 for an example from Abdiakamalov et al. [15]. Several authors (e.g., [22, 44]) have argued that the $\alpha = -1$ scaling observed in 3D simulations could be due to the physical nature of the postshock turbulent flow that deviates significantly from the assumptions of Kolmogorov turbulence. However, this is unlikely on the basis of the argument we presented above. Furthermore, a scaling with $\alpha = -1$ is unphysical because it would predict infinite turbulent kinetic energy in the limit of infinite resolution and zero viscosity.

Abdiakamalov et al. [15] argued that a common issue in these studies is that the resolution requirements for the recovery of an inertial range had been severely underestimated. Their interpretation is corroborated by the results of local simulations in periodic cubic domains, which showed that resolutions between 512^3 and 1024^3 are needed to recover an inertial range [63, 73, 77]. In contrast, typical global 3D CCSN simulations have resolutions roughly equivalent to those of a 64^3 local simulation [15].

In the light of local simulation results, Abdiakamalov et al. [15] suggested that the ℓ^{-1} spectra found by [15, 21, 22, 44] are the result of the so-called bottleneck effect [78–82]. This is a phenomenon arising because of the indirect influence of the (numerical) viscosity on the dynamics at large scale, which results in a build up of energy at wavenumbers close to the dissipation region. The presence of a numerical bottleneck effect is also likely to result in an artificially large ratio $\epsilon_{\text{turb}}/\epsilon_{\text{th}}$, which would create more favorable conditions for the explosion, as tentatively confirmed by Abdiakamalov et al. [15].

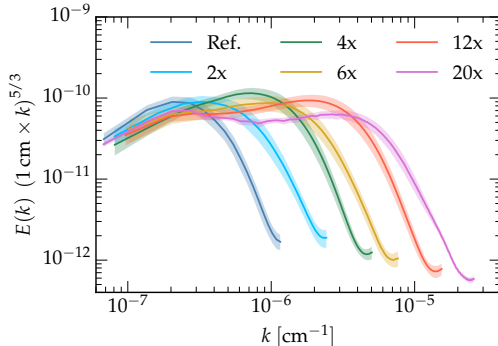


Figure 5. Compensated velocity power-spectra at increasing resolutions in 3D, semi-global, parameterized, neutrino-driven convection simulations. As the resolution is increased, the turbulent specific kinetic energy spectrum approaches the $k^{-5/3}$ slope predicted by Kolmogorov’s theory. Reprinted from D. Radice, C. D. Ott, E. Abdiakamalov, S. M. Couch, R. Haas, and E. Schnetter, *Neutrino-Driven Convection in Core-Collapse Supernovae: High-Resolution Simulations*, The Astrophysical Journal **820**, 76 (2016) [18]. © AAS. Reproduced with permission.

In this context, the $\ell^{-5/3}$ spectra from Hanke et al. [37] and Handy et al [68] might be interpreted as arising from a misidentification of the dissipation range and inertial ranges. Indeed, the spectra from Hanke et al. [37] appear to become shallower with increasing resolution. This would be expected if the putative inertial range with logarithmic slope $-5/3$ was actually a part of the exponentially decaying dissipation range.

More recently, Radice et al. [18] performed a very extensive resolution study of a parameterized neutrino-driven convection model. Their results are reproduced in Fig. 5. They found shallow velocity power spectra at their coarsest resolution, which was intermediate between the medium and the high resolution of Hanke et al. [37]. As they increased the resolution they eventually recovered Kolmogorov scaling, but only at a resolution $\simeq 16$ times higher than the highest resolution of Hanke et al. [37]. These results confirmed the interpretation by Abdiakamalov et al. [15] of the k^{-1} spectra seen in many simulations as being due to the insufficient resolution and provided solid numerical evidence for Kolmogorov’s phenomenology in neutrino-driven convection.

3. SASI-Generated Turbulence

The standing accretion shock instability (SASI) was discovered by Blondin et al. [9], who performed simplified 2D hydrodynamic simulations of stalled (“standing”) accretion shocks. They found that the stalled shock develops an oscillatory instability dominated by an (in terms of spherical harmonics) $\ell = 1$ “sloshing” mode. Later studies in 3D showed the prevalence of an azimuthal $m = 1$ spiral mode (e.g., [15, 22, 38, 41, 83–85]), which is enhanced by rotation (e.g., [86–88]).

In a series of papers [10, 14, 35, 59, 89–91], Foglizzo and colleagues identified SASI as an advective-acoustic instability (though see [92, 93] for a purely acoustic interpretation). In the advective-acoustic scenario depicted in Fig. 3, a small entropy or vorticity perturbation enters through the shock and is advected with the subsonic

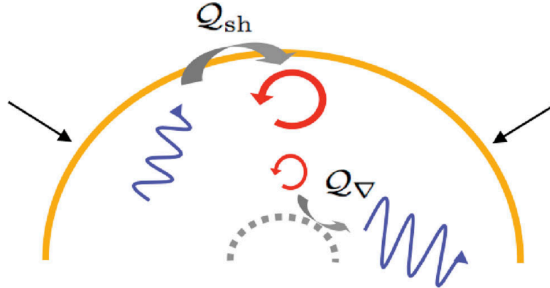


Figure 6. Schematic representation of the advective-acoustic instability underlying SASI. An entropy/vorticity perturbation is created at the shock front (orange half-circle) by the accretion flow. This perturbation is advected purely radially (red) to the edge of the protoneutron star (indicated by a dashed gray half-circle). There, it is strongly decelerated and converted into an upward pressure perturbation (i.e., acoustic wave) that has radial and transverse components (blue). Reprinted from J. Guilet & T. Foglizzo, *On the linear growth mechanism driving the standing accretion shock instability*, Monthly Notices of the Royal Astronomical Society **421**, 546 (2012) [91], © J. Guilet & T. Foglizzo. Reproduced with permission.

accretion flow toward the PNS. At the steep density gradient marking the PNS edge, it is decelerated, causing an outward propagating pressure (i.e., acoustic) wave with radial and transverse components.

In the non-linear regime of SASI, its oscillations reach large amplitudes and cause large spatially and temporally varying expansions and recessions of the shock front. The postshock entropy depends on the preshock velocity in the frame of the shock. The smaller the shock radius, the higher the preshock velocity and the higher the postshock entropy. Hence, SASI-driven variations in the shock radius lead to radial entropy gradients from which turbulent convection grows [35, 67, 94, 95]. Because of the lateral and azimuthal SASI shock motions, the radial preshock accretion flow impacts the shock at an oblique angle, leading to deflection and large non-radial velocity components. In the highly non-linear regime, non-radial streams from different phases of a SASI cycle collide, forming shear-regions, secondary shocks, and supersonic accretion funnels [35, 94, 96]. All these non-linear SASI features create conditions susceptible to turbulence and simulations show that fully turbulent (i.e., as turbulent as permitted by the employed resolution) postshock flow can develop from SASI even in CCSN cores that are initially stable to neutrino-driven convection (e.g., [35, 41, 67, 97]).

In 2D/3D hydrodynamic simulations, SASI is observed to saturate in strength/amplitude at the same time when the aforementioned non-linear flow features appear. Guilet et al. [95] analyzed the saturation behavior of SASI and proposed that saturation sets in when a parasitic instability is able to grow fast enough to compete with SASI by impeding the advective-acoustic cycle. They found that both the Rayleigh-Taylor instability (growing on entropy gradients) and the Kelvin-Helmholtz instability (growing in shear flows) can act as such a parasitic instability, but that the Rayleigh-Taylor instability may be the dominant saturation agent. In any case, both parasitic instabilities are well known to result in turbulent flow. This suggests that turbulence is a natural consequence of SASI, which is confirmed by simulations (e.g., [15, 22, 35, 67]).

Extensive research went into understanding the interplay of SASI and neutrino-driven convection, often with a focus on the question of which of the two instabilities is dominant in CCSNe. Because of the advective nature of the postshock CCSN flow, neutrino-driven convection can grow only if seed perturbations are large enough, the entropy gradient is steep enough, and/or the advection timescale is long enough (cf. Section 2.1, Eq. 2, and [14, 35]). SASI growth, on the other hand, is fastest if the advection timescale is short [14, 35]. CCSN simulations with conditions in which neutrino-driven convection grows fast and is strong and sustained do not appear to develop large-amplitude SASI (e.g., [15, 22, 43, 45]). In other simulations, e.g., those in which neutrino heating is weak or that use a progenitor with a particularly high accretion rate (e.g., [15, 22, 38]), neutrino-driven convection may fail to develop or may be present only temporarily. In these scenarios, SASI eventually dominates.

While turbulence appears to be a natural consequence of both instabilities, it remains to be clarified if SASI-induced turbulence is different in character from neutrino-driven turbulent convection. If it is related predominantly to entropy gradients and the Rayleigh-Taylor instability [35, 95], then its properties may be expected to be similar to turbulence resulting from neutrino-driven convection. This is supported by the turbulence analyses of recent detailed 3D CCSN simulations with SASI (e.g., [15, 22]). On the other hand, Endeve et al. [67] found in their 3D simulations that SASI-induced turbulence is driven predominantly by shear flows and is partially supersonic. However, Endeve et al.’s focus was on turbulent magnetic field amplification and they employed an idealized setup that left out much of the essential CCSN microphysics. More work in 3D with high-resolution full-physics simulations will be needed to fully characterize SASI-induced turbulence.

4. Pre-Supernova Turbulence

4.1. Turbulent Convection in Advanced Burning Stages

Most CCSN simulations start at the onset of the collapse of perfectly spherically-symmetric cores, computed using 1D stellar evolution codes. These employ effective treatments of convective mixing and overshooting, e.g., [23, 24, 98], that can account for some of the effects of convection, especially over secular timescales. However there are still important uncertainties associated with the use of these prescriptions, partly because turbulent convection in stellar interiors is still not completely understood, see e.g., [64, 99–108], for some recent works.

A more immediate concern for CCSN modelers is the fact that one-dimensional stellar evolution codes cannot predict the properties of non-spherical perturbations of the progenitor present at the onset of collapse. Convective velocities during advanced burning stages immediately prior to collapse could reach hundreds of kilometers per second [103, 106, 108]. Convection, as well as gravity waves excited in the iron core during silicon shell burning [109], will be frozen in the collapsing core after the onset of collapse. They will be amplified as they cross the shock (Sec. 4.2), and they may play an important role in triggering explosions (Sec. 5).

4.2. The Growth of Seed Perturbations in the Accretion Flow

In the process of stellar core-collapse, the convective flow in nuclear burning shells undergoes profound evolution during its journey towards the shock. In the absence of

nuclear burning and dissipative processes, the specific entropy of the flow is conserved, while the convective velocities increase due to conservation of angular momentum. If present, nuclear burning should in principle amplify convection, although the degree of amplification is limited if the collapse timescale is shorter than the convective turnover timescale. The dissipative processes should do the opposite. The vorticity waves, which have solenoidal velocity field, perturb the isodensity contours of the collapsing star, leading to the emission of powerful pressure waves [62]. Entropy fluctuations also generate pressure waves as they accrete in a converging flow (e.g, [110–112]).

The evolution of hydrodynamic perturbations in accretion flows has been studied in a number of works (e.g., [110, 112–116]). A general convective flow can be decomposed into the three physical modes: acoustic, vorticity, and entropy waves (e.g., [117]). Kovalenko & Eremin [110] studied the evolution of all these three modes for Bondi accretion. Using linearized hydrodynamics equations, they obtained simple analytical relations in the limit $r \rightarrow 0$ for the scaling of perturbation amplitudes with radius. In particular, for $\ell > 0$ acoustic and vorticity modes in the regime of supersonic mean flow, they find

$$\frac{\delta\rho}{\rho} \propto 2\ell(\ell+1)r^{-1/2}, \quad (19)$$

$$\frac{\delta v_r}{v_r} \propto \ell(\ell+1)r^{(4-3\gamma)/4}, \quad (20)$$

$$\frac{\delta v_\perp}{v_r} \propto r^{-1/2}, \quad (21)$$

$$\frac{\delta v_{\text{rot}}}{v_r} \propto r^{-1/2}, \quad (22)$$

where γ is the adiabatic index of the gas, ρ and v_r are unperturbed values of density and radial velocity, while $\delta\rho$, v_\perp , and v_{rot} are the perturbations of density and angular components of velocity, respectively. Lai & Goldreich [113] found similar relations for perturbations in collapsing clouds in the same $r \rightarrow 0$ limit.

Takahashi & Yamada [115] performed an analysis of the evolution of infalling perturbations in spherical supersonic Bondi accretion without imposing the $r \rightarrow 0$ limit and obtained the following scaling relations

$$\frac{\delta\rho}{\rho} \propto \ell r^{-(5-3\gamma)/4}, \quad (23)$$

$$\frac{\delta v_r}{v_r} \propto \ell r^{(5-3\gamma)/4}, \quad (24)$$

$$\frac{\delta v_\perp}{v_r} \propto \text{const}, \quad (25)$$

$$\frac{\delta v_{\text{rot}}}{v_r} \propto \ell r^{-1/2}, \quad (26)$$

These are somewhat different from corresponding scaling relations in [110, 113] and parts of the differences stem from the $r \rightarrow 0$ limit imposed in these works. A common limitation shared by these works is that they either consider only the supersonic region of accretion [113, 115] or only either supersonic or subsonic solutions of the Bondi accretion [110]. In CCSNe, the convective Si/O burning shells initially reside in subsonic region and gradually propagate into supersonic region. A detailed analysis of the evolution of convective perturbations from the subsonic to the supersonic regime,

including the effects of possible nuclear burning and turbulent dissipation, is currently lacking in the literature.

Müller et al. [116] performed supernova simulations of a 3D $18M_{\odot}$ progenitor model. They observed that, prior to collapse, the convective motion in the O shell mostly consists of solenoidal velocity field, while the density perturbations remains small. However, by the time the O shell reaches the shock, they observed strong density perturbations with amplitude $\delta\rho/\rho \simeq 0.1$ and peak angular wavenumber of $\ell \simeq 2$ with. They found that the spatial spectrum of the density perturbations prior to shock-crossing is very similar to that of the turbulent Mach number in the O shell prior to collapse. More specifically, for the normalized time-averaged spectrum of density perturbation, they found

$$\frac{\hat{\rho}_\ell}{\hat{\rho}_0} \simeq 0.5\hat{\mathcal{M}}_{r,\ell}, \quad (27)$$

where $\hat{\mathcal{M}}_{r,\ell}$ is the spectrum of the Mach number of radial velocity in the middle of the O shell (see their equation 6). Such as simple relation between the spectrum of the velocity perturbation in the oxygen shell and that of density perturbations just ahead of the shock has not been established by the above studies of the evolution of perturbations in Bondi accretion. This discrepancy may stem from the fact that the perturbative studies consider only the supersonic regime of collapse and use stationary Bondi flow, which does not account for exact density gradients in CCSN progenitors (see [116] for in-depth discussion).

5. Turbulence Shock Interaction

5.1. Numerical Results

Couch & Ott [21] were the first to show the impact of the accretion of perturbations in simulations. They considered the $15M_{\odot}$ progenitor from Woosley & Heger [118], which they evolved in 3D. They performed simulations either with the original, unperturbed, progenitor structure, or with velocity perturbations. They found that the accretion of perturbations enhances the turbulent kinetic energy in the gain region, especially at large scales. This has a number of beneficial effects for the explosion, as discussed in Sec. 2.2, and, in the case of the simulations of [21], it was sufficient to trigger an explosion in an otherwise failing model.

Müller & Janka [62] further explored the impact of perturbations in the accretion flow in 2D axisymmetric simulations. They systematically studied the effects of the character and angular scale of the perturbations. They found that in the case of velocity perturbations, low-order modes ($\ell = 1$ or $\ell = 2$) are the most effective in triggering explosions. Müller & Janka [62] quantified the impact of perturbations in terms of the critical neutrino luminosity and found a decrease of up to 10% for large-scale velocity perturbations. Density perturbations were also found to be very effective. However, a significant impact was found only for large perturbations, corresponding to pre-collapse turbulent Mach numbers of $\gtrsim 0.3$, which might be present only in a small fraction of progenitors [108].

In their analysis of the effects of perturbations on the post-shock turbulence, Müller & Janka [62] emphasized the role of the directionally-dependent modulation of the accretion rate ahead of the shock. However, analytic studies ([119]; Sec. 5.2) have shown that the effects of shock-turbulence interaction in CCSNe have a rather

complex phenomenology and that their effectiveness depends on the relative phase of entropy and vorticity perturbations accreted through the shock. In any case, both simulations and analytic theory suggest that the effect of perturbations depends on their detailed nature. This motivates the development of well motivated perturbed progenitor models.

Chatzopoulos et al. [120] developed a systematic method to characterize pre-collapse asphericities in CCSN progenitors. They proposed a method to extract characteristic properties of convection from multi-dimensional simulations of advanced burning stages in a way that allows them to be injected in otherwise spherical progenitor models at the verge of core collapse. More recently, Couch et al. [103] and Müller et al. [106, 116] simulated, for the first time, CCSN progenitors that were self-consistently evolved in multi-D in the last minutes prior to collapse.

Couch et al. [103] studied a $15-M_{\odot}$ progenitor. They self-consistently simulated the last few minutes of Si-burning, the collapse of the iron core, and the subsequent core bounce and explosion. They used a reduced 21-isotope nuclear network and a neutrino leakage scheme with parametrized heating. As a baseline for comparison, they re-simulated the collapse, bounce, and subsequent evolution of the same iron-core after angle averaging. They found that (non-spherical) turbulent fluctuations produced during Si burning resulted in an earlier and more energetic explosion. A possible caveat of this first study, however, is that Si burning was simulated only in an octant (assuming reflection symmetry across the coordinate planes). This prevented the appearance of convective cells with large angular scale, which seem to be the most effective for triggering explosions [62]. Consequently, the effects of perturbations might be even larger than found by Couch et al. [103].

Müller et al. [106, 116] considered instead an $18-M_{\odot}$ progenitor. They simulated the last ~ 5 minutes of evolution of the oxygen-burning shell in 4π (but excised most of the Fe/Si core of the star) [106]. The resulting progenitor was subsequently evolved in 3D with their fast multi-group transport method [62]. They found that perturbations determined the outcome of core collapse: while the progenitor with perturbations exploded ~ 0.3 seconds after bounce, the spherically-averaged progenitor did not explode within the end of their simulation (0.625 seconds after bounce). A third progenitor, obtained with an artificially reduced burning rate resulting in smaller convective velocities prior to collapse, exploded at ~ 0.5 seconds after bounce.

5.2. Analytical Results

5.2.1. Linear Analysis of Shock-Turbulence Interaction. Abdikamalov et al. [119] studied the impact of pre-shock perturbations on the evolution of the shock and post-shock flow using a linear perturbation theory known as the linear interaction analysis (LIA) (e.g., [121]). In the LIA, the flow is decomposed into mean and fluctuating parts. The unperturbed shock is assumed to be planar and the mean flow is assumed to be uniform in space. While these are approximations, the strength of the LIA lies in its simplicity, which allows one to obtain deep insight into the physics of shock-turbulence interaction (e.g., [121]). Furthermore, in its regime of applicability, when the turbulent Mach number of the perturbations ahead of the shock is small, the LIA shows excellent agreement with high-resolution numerical simulations [122].

In the LIA, the mean flow obeys the usual Rankine-Hugoniot conditions, while the fluctuations obey the linearized version of the jump conditions. The upstream flow completely determines the downstream flow via these conditions (e.g., [123–127]). The

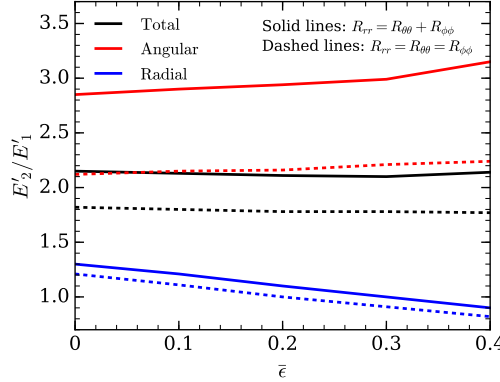


Figure 7. The amplification of turbulent kinetic energy at shock crossing for incoming incident waves as a function of dimensionless nuclear dissociation parameter. The latter characterizes the strength of nuclear dissociation at the shock, larger values of $\bar{\epsilon}$ corresponding to stronger dissociation [55, 128]. The black lines show the amplification of the total kinetic energy, while blue and red lines show the amplifications of radial and angular components of kinetic energy. The solid lines represent anisotropic turbulence characterized by the relation $R_{rr} = R_{\theta\theta} + R_{\phi\phi}$, while the dashed lines represent fully isotropic turbulence. The Mach number of the pre-shock mean flow is assumed to be 5. Reprinted from E. Abdikamalov, A. Zhaksylykov, D. Radice, and S. Berdibek, *Shock-turbulence interaction in core-collapse supernovae*, Monthly Notices of the Royal Astronomical Society **461**, 3864 (2016) [119], © E. Abdikamalov, A. Zhaksylykov, D. Radice, and S. Berdibek. Reproduced with permission.

perturbations can be decomposed into vorticity, entropy, and acoustic modes, each of which evolve independently at the linear order [117]. With this decomposition, the LIA formalism can be applied to each mode individually. The results can then be integrated to get the full depiction of shock-turbulence interaction to linear order.

Abdikamalov et al. [119] considered incoming field of vorticity and entropy waves. When vorticity and/or entropy waves hit a shock, they generate a downstream field of vorticity, entropy, and acoustic waves. Abdikamalov et al. [119] showed that the kinetic energy of fluctuations in the post-shock region is almost entirely due to vorticity waves, with acoustic waves contributing only $\lesssim 2\%$ of the total kinetic energy. They found that the total kinetic energy of turbulent fluctuations is amplified by a factor of ~ 2 at shock crossing. The angular component is amplified by a factor of ~ 3 , while the radial component does not undergo significant amplification (cf. Fig 7).

5.2.2. Impact on the Explosion Condition The impact of the progenitor asphericities on the explosion condition has been estimated analytically using the concept of the critical (i.e., minimum) neutrino luminosity necessary to drive an explosion [62, 106, 119]; see Nagakura et al. [129] for a possible alternative approach. In the absence of non-radial motion in the gain region, the critical luminosity can be estimated as [130]

$$(L_\nu E_\nu^2)_{\text{crit}} \propto (\dot{M} M)^{3/5} r_{\text{gain}}^{-2/5}, \quad (28)$$

which is approximately equivalent to condition $\tau_{\text{adv}}/\tau_{\text{heat}} \gtrsim 1$, where τ_{adv} and τ_{heat} are the timescales of advection and heating in the gain region, and r_{gain} is the radius

at which the net neutrino heating becomes positive [130]. The effect of post-shock turbulence can be included as an isotropic pressure contribution (cf. Eq. 10), which leads to a lower critical luminosity [62]:

$$(L_\nu E_\nu^2)_{\text{crit}} \propto (\dot{M} M)^{3/5} r_{\text{gain}}^{-2/5} \left(1 + \frac{4\langle \mathcal{M}'_2^2 \rangle}{3}\right)^{-3/5}, \quad (29)$$

where $\langle \mathcal{M}'_2^2 \rangle$ is the average Mach number of the turbulent flow in the post-shock region. The pre-shock fluctuations cross the shock and contribute to \mathcal{M}'_2 in the post-shock region. The reduction of the critical luminosity due to this “direct injection” of kinetic energy can be estimated as [119]

$$\frac{\Delta L_{\text{crit}}}{L_{\text{crit}}} \simeq \frac{4}{5} \frac{E'_{\text{a},2}}{E'_{\text{a},1}} \frac{\langle c_{\text{s},1}^2 \rangle}{\langle c_{\text{s},2}^2 \rangle} \langle \mathcal{M}'_1^2 \rangle, \quad (30)$$

where $\langle c_{\text{s},1}^2 \rangle$ and $\langle c_{\text{s},2}^2 \rangle$ are the sound speeds in the pre-shock and post-shock regions. In the absence of turbulent dissipation, the ratio $E'_{\text{a},2}/E'_{\text{a},1}$ of the turbulent kinetic energies in the immediate post-shock and pre-shock regions can be obtained from the LIA formalism [119]. For typical parameters of the accretion shock, and assuming anisotropic turbulence with $R_{rr} = R_{\theta\theta} + R_{\phi\phi}$, Eq. (30) yields

$$\frac{\Delta L_{\text{crit}}}{L_{\text{crit}}} \simeq 0.6 \langle \mathcal{M}'_1^2 \rangle, \quad (31)$$

The turbulent Mach number in nuclear burning shells is ~ 0.1 (e.g., [106, 108]). The conservation of angular momentum dictates that, in the absence of turbulent dissipation and nuclear burning, the Mach number of non-radial fluctuations should increase as $\propto r^{(3\gamma-7)/4}$ during accretion [110, 113]. Accordingly, if convective shells accrete from ~ 1500 km toward the shock at ~ 200 km, the turbulent Mach number increases by a factor of ~ 4.5 to ~ 0.45 . Compared to the case with no pre-collapse perturbations, this leads to a reduction of the critical luminosity by $\sim 12\%$.

Recent 3D neutrino-hydrodynamics simulations of the $18M_\odot$ progenitor model infer a reduction of $\sim 20\%$ in the critical luminosity [116], which is significantly larger than the above estimate. This suggests that the direct injection of kinetic energy plays a sub-dominant role in triggering an explosion [62]. An additional contribution should come from buoyant driving of convection in the post-shock region.

An alternative approach that approximately includes this effect was presented by [106]. Their calculation is based on the observation that pre-collapse perturbations with Mach number \mathcal{M} generate density perturbations with relative amplitude of $\sim \mathcal{M}$ by the time they reach the shock. After crossing the shock, these density perturbations drive turbulent convection in the gain region as a result of the work by buoyancy. The reduction of the critical luminosity can be estimated as [106]

$$\frac{\Delta L_{\text{crit}}}{L_{\text{crit}}} \simeq 0.47 \frac{\mathcal{M}}{\ell \eta_{\text{acc}} \eta_{\text{heat}}}, \quad (32)$$

where ℓ is the peak angular wave number of the perturbations, η_{heat} is the neutrino-heating efficiency, η_{acc} is the efficiency of conversion of accretion energy into electron-flavor neutrino emission. Recently, Huete et al. [127] pointed out the importance of entropy perturbations generated by the interaction of the supernova shock with vorticity waves originating from nuclear burning shells. These perturbations are associated with density fluctuations, which become buoyant and contribute to the

turbulent convection in the gain region. Depending on problem parameters, the resulting reduction in the critical luminosity was estimated to be

$$\frac{\Delta L_{\text{crit}}}{L_{\text{crit}}} \simeq (0.68 - 0.96) \times \frac{\mathcal{M}}{\ell \eta_{\text{acc}} \eta_{\text{heat}}}. \quad (33)$$

For typical values of $\eta_{\text{heat}} \simeq 0.1$, and $\eta_{\text{acc}} \simeq 2$, this implies a $\sim 17 - 24\%$ reduction of the critical luminosity for $\mathcal{M} \simeq 0.1$ and $\ell = 2$. This is roughly in line with the results of 3D neutrino-hydrodynamics simulations of [116].

5.2.3. Normal Mode Analysis. Takahashi et al. [131] studied the influence of upstream perturbations on convective and SASI modes. Their model is based on the solution of linearized hydrodynamic equations in the post-shock region with a boundary condition at the shock that mimics pre-shock perturbations. They considered a stationary spherically symmetric background model with neutrino heating. They applied perturbations of the specific form

$$\frac{\delta \rho}{\rho} = \sin(\omega_{\text{up}} t + \phi), \quad (34)$$

$$\frac{\delta v}{v_r} = -0.5 \sin(\omega_{\text{up}} t + \phi), \quad (35)$$

$$\frac{\delta \epsilon}{\epsilon} = \sin(\omega_{\text{up}} t + \phi), \quad (36)$$

Here, ω_{up} is the frequency, ϕ is the phase of the perturbation, and ϵ is the specific internal energy. The linearized equations for the perturbation field are then solved using the Laplace transform, which allowed them to calculate the frequencies and growth rates of the SASI and convection modes under the influence of these perturbations. Takahashi et al. [131] systematically studied the dependence on frequency and phase of the perturbations and showed that resonant amplification of SASI and convection can occur when both the frequency and the growth rate of upstream perturbations match those of the intrinsic SASI and convective modes, respectively. Due to this rather stringent requirement, such resonances are unlikely to occur in CCSNe. However, they found that the amplitudes of intrinsic modes become larger by a factor of $\lesssim 10$ when the frequency of the upstream perturbations is close to that of the intrinsic SASI mode or to the growth rate of convection. This suggests that accreted perturbations might efficiently drive SASI and/or convection to nonlinear amplitudes.

6. Protoneutron Star Convection

The gain region is not the only area with convective overturn active after core bounce. Immediately after neutrino shock breakout, the weakening shock leaves behind a negative entropy gradient, which rapidly develops convection [51, 132–134]. However, this initial convective overturn subsides within ~ 10 ms [135], as the unstable entropy gradient is erased by neutrino heating and convective mixing.

Later, neutrino losses from the outer layers of the PNS establish negative entropy and lepton number gradients at densities above $\sim 10^{13} \text{ g cm}^{-3}$. A second, much longer, period of convective overturn develops because of the presence of these gradients [12, 51, 135, 138, 139]. The region of the PNS that is unstable to convection depends on the nuclear EOS, which can be seen from the thermodynamic derivatives

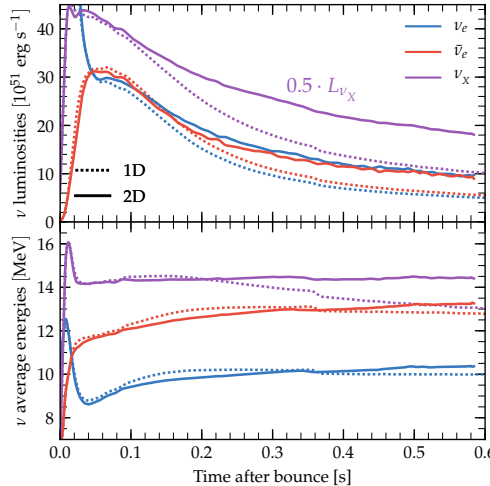


Figure 8. Neutrino luminosity (top panel) and average energies (bottom panel) at 10,000 km as a function of time for the ONeMg electron-capture supernova progenitor of Nomoto [136, 137] computed by Radice et al. [8] with their “Baseline” setup. Here, “ ν_X ” denotes the sum of all the heavy-lepton neutrinos. Since this progenitor model explodes in 1D and 2D, the neutrino luminosities in both cases are only due to the cooling PNS and there is no contribution from the accretion luminosity. Consequently, the differences between 1D and 2D are attributable to the effect of PNS convection.

appearing in the Brunt-Väisälä frequency (see Equation 1). In general, $(\partial p / \partial s)_{\rho, Y_e}$ is positive, so negative entropy gradients drive instability. On the other hand, $(\partial p / \partial Y_e)_{\rho, s}$ can be negative under the conditions encountered in the outer layers of the PNS. Here, the pressure is mainly determined by high-density, interacting neutron gas and the degenerate electron gas. If the neutron gas provides the dominant contribution, reducing the electron fraction increases the pressure. This implies the negative lepton gradients in the outer layers of the PNS can have a stabilizing influence for some EOSs and the convectively unstable region will depend on the nuclear EOS. This second phase of PNS convection can persist for many seconds and leave a detectable signature in the neutrino signal from the cooling PNS [140].

Early 2D calculations with energy-integrated neutrino transport [135] suggested that the convective transport of energy and lepton number from the PNS core toward the neutrinospheres could play an important role in the dynamics of the explosion, since it resulted in an increase of the neutrino luminosities by up to a factor two. However, the first 2D simulations with energy-dependent neutrino transport found a very different picture [138, 139]. In these models, PNS convection was buried deep below the neutrinospheres by large stabilizing entropy gradients interior and exterior to it. Accordingly, PNS convection could only provide a $\sim 15\%$ to $\sim 30\%$ increase of the neutrino luminosities in the first 300 ms after bounce [138, 139].

More recently, Radice et al. [8] pointed out that, over longer timescales, the contraction of the PNS proceeds to the point that its surface comes into contact with the PNS convection region. Afterward, they found differences in the neutrino luminosities as large as a factor two between their 1D and 2D calculations, which they attributed to PNS convection. Fig. 8 shows the neutrino luminosities and average

energies from their simulation of the $8.8 M_{\odot}$ (zero-age main sequence) progenitor from Nomoto [136, 137]. Since this progenitor explodes already 50 milliseconds after bounce even in 1D calculations, the differences in the neutrino luminosities are genuinely related to PNS convection and are not due to differences in the accretion flow. The figure demonstrates the $\sim 2 \times$ boost of the luminosities, as well as a slight increase in the average neutrino energies. A similar enhancement of the heavy-lepton neutrino luminosities was also found by O'Connor & Couch [27]. However, they did not find a correspondingly large boost of the electron-type neutrino luminosity, presumably because the smaller luminosities in their 1D calculations were offset by the larger accretion luminosities.

Other consequences of PNS convection are the reduced contraction rate of the PNS [8, 138] and the launching of gravity waves in the stably stratified region above it [139]. The first effect is mostly negative for the prospects of the explosion, since it results in a reduction of the average neutrino energies by several percent. This reduction, in turn, reduces the coupling between the neutrinos and the matter behind the shock. The second effect is, instead, positive, since gravity waves transport energy out of the core and release it near the surface of the PNS. This energy is subsequently radiated as neutrinos and, in part, reabsorbed in the gain layer behind the shock.

The Ledoux-stable region above the inner convection layer has received significant attention before the advent of multidimensional simulations with spectral neutrino transport. Wilson and Mayle [141, 142] suggested that a doubly diffusive instability might operate in this region. They argued that if a parcel of neutron rich matter is displaced toward the center of the PNS, then it would thermally equilibrate on a very short timescale. However, because of the net cancellation of the interaction with electron and anti-electron neutrinos, this material would still be more neutron rich than the surroundings. As a result of the smaller electron pressure, the fluid blob would keep on sinking, forming a so-called neutron finger. Convective overturn would then rapidly develop and transport lepton number and heat from the core of the PNS all the way to the neutrinospheres. This would significantly boost the neutrino luminosities. Indeed, their 1D models with an effective prescription of the neutron-finger instability successfully exploded [142].

However, Bruenn & Dineva [143] later pointed out that a radially displaced fluid element below the neutrinospheres would reach equilibration mostly because of the emission of low energy electron-type neutrinos. The reason is, on the one hand, that heavy-lepton neutrinos are not effective at transporting heat and, on the other hand, that high energy electron-type neutrinos would be trapped due to their small mean free path. Consequently, the displaced fluid element would achieve lepton-number re-equilibration before cooling down to the ambient temperature, and the neutron-finger instability should not develop. This has since been confirmed by multidimensional simulations, which found no evidences for the neutron finger or other doubly diffusive instabilities [144] in the PNS [138, 139].

7. Magnetic Effects

Magnetic fields can play an important role in the CCSN explosion mechanism. In rapidly rotating progenitors, they act as an agent powering jet-like outflows by extracting rotational energy, e.g., [145–147]. The necessary magnetar-strength field ($\sim 10^{15}$ G) can be obtained via flux-compression and winding from strongly magnetized progenitor cores [148] or via magnetoturbulence [149–151] in the shear

layer surrounding the PNS. While many studies have focused on magnetic fields in rapidly rotating progenitors, the impact of magnetic fields in slowly or non-rotating progenitors has so far received limited attention in the literature.

Endeve et al. [67, 152] investigated the magnetic field amplification by the SASI in 2D axisymmetric and 3D simulations. They found that SASI-driven turbulence in the post-shock region amplifies magnetic field exponentially fast by multiple orders of magnitude and can account for neutron star magnetic fields of $\sim 10^{14}$ G or more in non-rotating progenitors. However, while the magnetic field amplification impacted the local flow properties in their simulations, they did not find a modification of the global dynamics.

Obergaulinger et al. [153] studied magnetic amplification and evolution of non-rotating magnetized CCSNe via 2D axisymmetric simulations. They considered a $15 M_{\odot}$ -progenitor augmented with a seed magnetic fields, of which they varied the initial strengths. They found that convection and the SASI amplify magnetic field in the gain region by up to a factor ~ 5 , which they explained in terms of the ratio between the advection and the eddy-turnover times. As a consequence of this modest amplification factor, they found weakly magnetized models, with pre-collapse fields smaller than 10^{12} G, to evolve very similarly to purely hydrodynamical models. Only in their 10^{12} G-model the magnetic field energy reached equipartition with the kinetic energy and was able to trigger a considerably earlier explosion.

Summarizing, extant studies on magnetized CCSNe are inconclusive concerning the role that magnetic fields can play in the explosion of slowly- or non-rotating progenitors. On the one hand, global qualitative changes in the dynamics have been reported only for very large pre-collapse fields. On the other hand, a quantitative impact on the flow is present even for realistic seed fields. Moreover, the simulations have been carried out so far only established a lower bound for the amplification factor of the magnetic fields. First, axisymmetric simulations significantly restrict the possibilities for magnetic field amplification, as illustrated by the anti-dynamo theorem [154], see also [155]. Second, 3D studies are limited in their resolution and may have not reached sufficiently high effective Reynolds numbers to fully capture the magnetic field amplification. Future studies that investigate magnetic fields amplification and their potential to alter the flow properties in 3D are needed to understand their role and impact for slowly or non-rotating CCSN progenitors.

8. Conclusions

Turbulence is an important component of the CCSN explosion mechanism. Turbulent convection during the last stages of nuclear burning creates perturbations that are then frozen in the collapsing gas after the onset of core collapse. These perturbations can seed fluid instabilities, such as the SASI or neutrino-driven convection, as they are accreted by the shock. The development of strong SASI and/or neutrino-driven convection, in turn, creates favorable conditions for the explosion. Convection inside the PNS can boost the neutrino luminosity and might in some cases contribute to shock revival. Finally, magnetic fields are expected to be amplified by convection and/or by other MHD instabilities, such as the magnetorotational instability (MRI), and might play an important role in the explosion.

Many of these important parts of the CCSN explosion mechanism puzzle have been pieced together in the past few years. However, this progress has been driven either by specialized/idealized simulations that addressed only one of these aspects

in isolation, or by means of simulations that ostensibly included all of the relevant physics, but lacked the numerical resolution necessary to capture all scales of the problem. Solving the CCSN explosion mechanism problem will necessarily require a way to bridge the gap between these two approaches. A possible way forward might be the development of subgrid-scale models for the effective treatment of turbulence in global simulations. This will be an object of our future work.

Acknowledgments

The authors acknowledge Adam Burrows, Jérôme Guilet, Roland Haas, Thierry Foglizzo, Bernhard Müller, Jeremiah W. Murphy, and Evan O'Connor for insightful discussion on the explosion mechanism of core-collapse supernovae. DR gratefully acknowledges support from the Schmidt Fellowship, the Sherman Fairchild Foundation and the Max-Planck/Princeton Center (MPPC) for Plasma Physics (NSF PHY-1523261). CDO is partially supported by NSF grant CAREER PHY-1151197. Work presented in this review benefitted from computer time allocations at NSF/NCSA Blue Waters (PRAC ACI-1440083), at the National Energy Research Scientific Computing Center (project m152), a DOE Office of Science User Facility supported by the Office of Science of the U.S. Department of Energy under Contract No. DE-AC02-05CH11231, and on the Texas Advanced Computing Center Stampede cluster under NSF XSEDE allocation TG-PHY100033.

References

References

- [1] Colgate S A and McKee C 1969 *Astrophys. J.* **157** 623
- [2] Bethe H A and Wilson J R 1985 *Astrophys. J.* **295** 14–23
- [3] Rampp M and Janka H T 2000 *Astrophys. J. Lett.* **539** L33
- [4] Liebendörfer M, Mezzacappa A, Thielemann F K, Messer O E B, Hix W R and Bruenn S W 2001 *Phys. Rev. D* **63** 103004
- [5] Thompson T A, Burrows A and Pinto P A 2003 *Astrophys. J.* **592** 434
- [6] Liebendörfer M, Rampp M, Janka H T and Mezzacappa A 2005 *Astrophys. J.* **620** 840
- [7] Sumiyoshi K, Yamada S, Suzuki H, Shen H, Chiba S and Toki H 2005 *Astrophys. J.* **629** 922
- [8] Radice D, Burrows A, Vartanyan D, Skinner M A and Dolence J C 2017 *ArXiv e-prints*: 1702.03927
- [9] Blondin J M, Mezzacappa A and DeMarino C 2003 *Astrophys. J.* **584** 971
- [10] Foglizzo T, Galletti P, Scheck L and Janka H T 2007 *Astrophys. J.* **654** 1006
- [11] Herant M 1995 *Phys. Rep.* **256** 117
- [12] Burrows A, Hayes J and Fryxell B A 1995 *Astrophys. J.* **450** 830
- [13] Janka H T and Müller E 1996 *Astron. and Astrophys.* **306** 167
- [14] Foglizzo T, Scheck L and Janka H T 2006 *Astrophys. J.* **652** 1436
- [15] Abdikamalov E, Ott C D, Radice D, Roberts L F, Haas R, Reisswig C, Mösta P, Klion H and Schnetter E 2015 *Astrophys. J.* **808** 70
- [16] Garnier E, Adams N and Sagaut P 2000 *Large Eddy Simulation for Compressible Flows* (Springer, Berlin, Germany)
- [17] Aubard G, Stefanin Volpiani P, Gloerfelt X and Robinet J C 2013 *Flow, Turbulence and Combustion* **91** 497–518
- [18] Radice D, Ott C D, Abdikamalov E, Couch S M, Haas R and Schnetter E 2016 *Astrophys. J.* **820** 76
- [19] Kraichnan R H 1967 *Phys. Fluids* **10** 1417
- [20] Lentz E J, Bruenn S W, Hix W R, Mezzacappa A, Messer O E B, Endeve E, Blondin J M, Harris J A, Marronetti P and Yakunin K N 2015 *Astrophys. J. Lett.* **807** L31
- [21] Couch S M and Ott C D 2015 *Astrophys. J.* **799** 5
- [22] Couch S M and O'Connor E P 2014 *Astrophys. J.* **785** 123

- [23] Paxton B, Bildsten L, Dotter A, Herwig F, Lesaffre P and Timmes F 2011 *Astrophys. J. Supp.* **192** 3
- [24] Paxton B, Cantiello M, Arras P, Bildsten L, Brown E F, Dotter A, Mankovich C, Montgomery M H, Stello D, Timmes F X and Townsend R 2013 *Astrophys. J. Supp.* **208** 4
- [25] Fryxell B, Olson K, Ricker P, Timmes F X, Zingale M, Lamb D Q, MacNeice P, Rosner R, Truran J W and Tufo H 2000 *Astrophys. J. Supp.* **131** 273
- [26] Dubey A, Reid L B, Weide K, Antypas K, Ganapathy M K, Riley K, Sheeler D and Siegal A 2009 *Parallel Comput.* **35** 512
- [27] O'Connor E and Couch S M 2015 *Submitted to Astrophys. J.*
- [28] Vincent A and Meneguzzi M 1991 *Journal of Fluid Mechanics* **225** 1
- [29] Janka H T, Hanke F, Hüdepohl L, Marek A, Müller B and Obergaulinger M 2012 *Prog. Th. Exp. Phys.* **2012** 01A309
- [30] Burrows A 2013 *Rev. Mod. Phys.* **85** 245
- [31] Janka H T, Melson T and Summa A 2016 *Annual Review of Nuclear and Particle Science* **66** 341–375
- [32] Müller B 2016 *Pub. Astron. Soc. Aus.* **33** e048
- [33] Chandrasekhar S 1939 *An Introduction to the Study of Stellar Structure*
- [34] Ledoux P 1947 *Astrophys. J.* **105** 305
- [35] Scheck L, Janka H T, Foglizzo T and Kifonidis K 2008 *Astron. and Astrophys.* **477** 931
- [36] Burrows A, Dolence J C and Murphy J W 2012 *Astrophys. J.* **759** 5
- [37] Hanke F, Marek A, Müller B and Janka H T 2012 *Astrophys. J.* **755** 138
- [38] Hanke F, Müller B, Wongwathanarat A, Marek A and Janka H T 2013 *Astrophys. J.* **770** 66
- [39] Fernández R, Müller B, Foglizzo T and Janka H T 2014 *Mon. Not. Roy. Astron. Soc.* **440** 2763
- [40] Iwakami W, Nagakura H and Yamada S 2014 *Astrophys. J.* **786** 118
- [41] Fernández R 2015 *Mon. Not. Roy. Astron. Soc.* **452** 2071–2086
- [42] Cardall C Y and Budiardja R D 2015 *Astrophys. J. Lett.* **813** L6
- [43] Ott C D, Abdikamalov E, Mösta P, Haas R, Drasco S, O'Connor E P, Reisswig C, Meakin C A and Schnetter E 2013 *Astrophys. J.* **768** 115
- [44] Dolence J C, Burrows A, Murphy J W and Nordhaus J 2013 *Astrophys. J.* **765** 110
- [45] Murphy J W, Dolence J C and Burrows A 2013 *Astrophys. J.* **771** 52
- [46] Couch S M 2013 *Astrophys. J.* **775** 35
- [47] Takiwaki T, Kotake K and Suwa Y 2014 *Astrophys. J.* **786** 83
- [48] Melson T, Janka H T and Marek A 2015 *Astrophys. J. Lett.* **801** L24
- [49] Melson T, Janka H T, Bollig R, Hanke F, Marek A and Müller B 2015 *Astrophys. J. Lett.* **808** L42
- [50] Roberts L F, Ott C D, Haas R, O'Connor E P, Diener P and Schnetter E 2016 *Astrophys. J.* **831** 98
- [51] Bethe H A 1990 *Rev. Mod. Phys.* **62** 801
- [52] Herant M, Benz W, Hix W R, Fryer C L and Colgate S A 1994 *Astrophys. J.* **435** 339
- [53] Burrows A and Goshy J 1993 *Astrophys. J. Lett.* **416** L75
- [54] Murphy J W, Ott C D and Burrows A 2009 *Astrophys. J.* **707** 1173
- [55] Fernández R and Thompson C 2009 *Astrophys. J.* **703** 1464
- [56] Marek A and Janka H T 2009 *Astrophys. J.* **694** 664
- [57] Fernández R 2012 *Astrophys. J.* **749** 142
- [58] Müller B, Janka H T and Marek A 2012 *Astrophys. J.* **756** 84
- [59] Yamasaki T and Yamada S 2007 *Astrophys. J.* **656** 1019
- [60] Murphy J W and Burrows A 2008 *Astrophys. J.* **688** 1159
- [61] Murphy J W and Meakin C 2011 *Astrophys. J.* **742** 74
- [62] Müller B and Janka H T 2015 *Mon. Not. Roy. Astron. Soc.* **448** 2141–2174
- [63] Radice D, Couch S M and Ott C D 2015 *Comp. Astrophys. Cosmol.* **2** 7
- [64] Arnett D, Meakin C and Young P A 2009 *Astrophys. J.* **690** 1715
- [65] Mabanta Q and Murphy J W 2017 *ArXiv e-prints:* 1706.0007
- [66] Murphy J W and Dolence J C 2017 *Astrophys. J.* **834** 183
- [67] Endeve E, Cardall C Y, Budiardja R D, Beck S W, Bejnood A, Toedte R J, Mezzacappa A and Blondin J M 2012 *Astrophys. J.* **751** 26
- [68] Handy T, Plewa T and Odrzywolek A 2014 *Astrophys. J.* **783** 125
- [69] Frisch U 1996 *Turbulence: The Legacy of A. N. Kolmogorov* (Cambridge University Press)
- [70] Peebles P J E 1993 *Principles of Physical Cosmology* (Princeton Univ. Press, Princeton, NJ, USA)
- [71] Couch S M and Ott C D 2013 *Astrophys. J. Lett.* **778** L7
- [72] Müller B and Janka H T 2014 *Astrophys. J.* **788** 82

- [73] Porter D H, Woodward P R and Pouquet A 1998 *Phys. Fluids* **10** 237
- [74] Benzi R, Biferale L, Fisher R T, Kadanoff L P, Lamb D Q and Toschi F 2008 *Phys. Rev. Lett.* **100** 234503
- [75] Goldreich P and Keeley D A 1977 *Astrophys. J.* **211** 934–942
- [76] Summa A, Janka H T, Melson T and Marek A 2017 *ArXiv e-prints: 1708.04154*
- [77] Sytine I V, Porter D H, Woodward P R, Hodson S W and Winkler K H 2000 *J. Comp. Phys.* **158** 225
- [78] Yakhot V and Zakharov V 1993 *Phys. D* **64** 379
- [79] She Z and Jackson E 1993 *Phys. Fluids* **5** 1526
- [80] Falkovich G 1994 *Phys. Fluids* **6** 1411–1414
- [81] Verma M K and Donzis D 2007 *J. Phys. A* **40** 4401
- [82] Frisch U, Kurien S, Pandit R, Pauls W, Ray S, Wirth A and Zhu J Z 2008 *Phys. Rev. Lett.* **101** 144501
- [83] Blondin J M and Mezzacappa A 2007 *Nature* **445** 58
- [84] Iwakami W, Kotake K, Ohnishi N, Yamada S and Sawada K 2008 *Astrophys. J.* **678** 1207
- [85] Fernández R 2010 *Astrophys. J.* **725** 1563
- [86] Iwakami W, Kotake K, Ohnishi N, Yamada S and Sawada K 2009 *Astrophys. J.* **700** 232
- [87] Nakamura K, Kuroda T, Takiwaki T and Kotake K 2014 *Astrophys. J.* **793** 45
- [88] Blondin J M, Gipson E, Harris S and Mezzacappa A 2017 *Astrophys. J.* **835** 170
- [89] Foglizzo T 2009 *Astrophys. J.* **694** 820
- [90] Sato J, Foglizzo T and Fromang S 2009 *Astrophys. J.* **694** 833
- [91] Guilet J and Foglizzo T 2012 *Mon. Not. Roy. Astron. Soc.* **421** 546
- [92] Blondin J M and Mezzacappa A 2006 *Astrophys. J.* **642** 401
- [93] Laming J M 2007 *Astrophys. J.* **659** 1449
- [94] Burrows A, Livne E, Dessart L, Ott C D and Murphy J 2006 *Astrophys. J.* **640** 878
- [95] Guilet J, Sato J and Foglizzo T 2010 *Astrophys. J.* **713** 1350
- [96] Burrows A, Livne E, Dessart L, Ott C D and Murphy J 2007 *Astrophys. J.* **655** 416
- [97] Müller B, Janka H T and Heger A 2012 *Astrophys. J.* **761** 72
- [98] Cox J P and Giuli R T 1968 *Principles of Stellar Structure* (New York: Gordon and Breach)
- [99] Meakin C A and Arnett D 2007 *Astrophys. J.* **667** 448
- [100] Viallet M, Meakin C, Arnett D and Mocák M 2013 *The Astrophysical Journal* **769** 1
- [101] Herwig F, Woodward P R, Lin P H, Knox M and Fryer C 2014 *Astrophys. J. Lett.* **792** L3
- [102] Woodward P R, Herwig F and Lin P H 2015 *Astrophys. J.* **798** 49
- [103] Couch S M, Chatzopoulos E, Arnett W D and Timmes F X 2015 *Astrophys. J. Lett.* **808** L21
- [104] Arnett W D and Meakin C 2016 *Reports on Progress in Physics* **79** 102901
- [105] Chatzopoulos E, Couch S M, Arnett W D and Timmes F X 2016 *Astrophys. J.* **822** 61
- [106] Müller B, Viallet M, Heger A and Janka H T 2016 *Astrophys. J.* **833** 124
- [107] Cristini A, Meakin C, Hirschi R, Arnett D, Georgy C, Viallet M and Walkington I 2017 *Mon. Not. Roy. Astron. Soc.* **471** 279–300
- [108] Collins C, Müller B and Heger A 2017 *ArXiv e-prints:1709.00236*
- [109] Goldreich P and Kumar P 1990 *Astrophys. J.* **363** 694–704
- [110] Kovalenko I G and Eremin M A 1998 *Mon. Not. Roy. Astron. Soc.* **298** 861–870
- [111] Foglizzo T and Tagger M 2000 *Astron. and Astrophys.* **363** 174–183
- [112] Foglizzo T 2001 *Astron. and Astrophys.* **368** 311–324
- [113] Lai D and Goldreich P 2000 *Astrophys. J.* **535** 402
- [114] Cao Y and Lou Y Q 2010 *Mon. Not. Roy. Astron. Soc.* **403** 491–495
- [115] Takahashi K and Yamada S 2014 *Astrophys. J.* **794** 162
- [116] Müller B, Melson T, Heger A and Janka H T 2017 *Mon. Not. Roy. Astron. Soc.* **472** 491–513
- [117] Kovasznay L S G 1953 *Journal of the Aeronautical Sciences* **20** 657–674
- [118] Woosley S E and Heger A 2007 *Phys. Rep.* **442** 269
- [119] Abdikamalov E, Zhaksylykov A, Radice D and Berdibek S 2016 *Mon. Not. Roy. Astron. Soc.* **461** 3864–3876
- [120] Chatzopoulos E, Graziani C and Couch S M 2014 *Astrophys. J.* **795** 92
- [121] Sagaut P and Cambon C 2008 *Homogeneous Turbulence Dynamics* (Cambridge University Press)
- [122] Ryu J and Livescu D 2014 *Journal of Fluid Mechanics* **756** R1
- [123] Mahesh K, Moin P and Lele S K 1996 The interaction of a shock wave with a turbulent shear flow Tech. Rep. TF-69 Thermosciences division, Department of Mechanical Engineering, Stanford University
- [124] Wouchuk J G, Huete Ruiz de Lira C and Velikovich A L 2009 *Phys. Rev. E* **79**(6) 066315
- [125] Huete C, Wouchuk J G and Velikovich A L 2012 *Phys. Rev. E* **85**(2) 026312

- [126] Huete C, Snchez A L and Williams F A 2013 *Physics of Fluids* **25** 076105
- [127] Huete C, Abdikamalov E and Radice D 2017 *Submitted to MNRAS, ArXiv e-prints: 1709.07363*
- [128] Fernández R and Thompson C 2009 *Astrophys. J.* **697** 1827
- [129] Nagakura H, Yamamoto Y and Yamada S 2013 *Astrophys. J.* **765** 123
- [130] Janka H T 2012 *Ann. Rev. Nuc. Par. Sci.* **62** 407
- [131] Takahashi K, Iwakami W, Yamamoto Y and Yamada S 2016 *Astrophys. J.* **831** 75
- [132] Epstein R I 1979 *Mon. Not. Roy. Astron. Soc.* **188** 305
- [133] Burrows A 1987 *Astrophys. J. Lett.* **318** L57–L61
- [134] Burrows A and Lattimer J M 1988 *Phys. Rep.* **163** 51–62
- [135] Burrows A and Fryxell B A 1993 *Astrophys. J. Lett.* **418** L33
- [136] Nomoto K, Sugimoto D, Sparks W M, Fesen R A, Gull T R and Miyaji S 1982 *Nature* **299** 803–805
- [137] Nomoto K 1984 *Astrophys. J.* **277** 791
- [138] Buras R, Janka H T, Rampp M and Kifonidis K 2006 *Astron. and Astrophys.* **457** 281
- [139] Dessart L, Burrows A, Livne E and Ott C D 2006 *Astrophys. J.* **645** 534
- [140] Roberts L F, Shen G, Cirigliano V, Pons J A, Reddy S and Woosley S E 2012 *Phys. Rev. Lett.* **108** 061103
- [141] Wilson J R and Mayle R W 1988 *Phys. Rep.* **163** 63
- [142] Wilson J R and Mayle R W 1993 *Phys. Rep.* **227** 97
- [143] Bruenn S W and Dineva T 1996 *Astrophys. J. Lett.* **458** L71
- [144] Bruenn S W, Raley E A and Mezzacappa A 2004 *ArXiv e-prints:0404099*
- [145] Burrows A, Dessart L, Livne E, Ott C D and Murphy J 2007 *Astrophys. J.* **664** 416–434
- [146] Takiwaki T and Kotake K 2011 *Astrophys. J.* **743** 30
- [147] Mösta P, Richers S, Ott C D, Haas R, Piro A L, Boydston K, Abdikamalov E, Reisswig C and Schnetter E 2014 *Astrophys. J. Lett.* **785** L29
- [148] Wheeler J C, Meier D L and Wilson J R 2002 *Astrophys. J.* **568** 807
- [149] Akiyama S and Wheeler J C 2005 *Astrophys. J.* **629** 414
- [150] Obergaulinger M, Cerdá-Durán P, Müller E and Aloy M A 2009 *Astron. and Astrophys.* **498** 241
- [151] Mösta P, Ott C D, Radice D, Roberts L F, Haas R and Schnetter E 2015 *Nature* **528** 376
- [152] Endeve E, Cardall C Y, Budiardja R D and Mezzacappa A 2010 *Astrophys. J.* **713** 1219
- [153] Obergaulinger M, Janka H T and Aloy M A 2014 *Mon. Not. Roy. Astron. Soc.* **445** 3169
- [154] Cowling T G 1933 *Monthly Notices of the Royal Astronomical Society* **94** 39–48
- [155] Brandenburg A and Subramanian K 2005 *Phys. Rep.* **417** 1–209